Study of Reducing Losses, Short-Circuit currents and Harmonics by Allocation of Distributed Generation, Capacitor Banks and Fault Current Limiters in Distribution grids

Lucas F. S**. Azeredo, Imene Yahyaoui*, Rodrigo Fiorotti**, Jussara F. Fardin**, Hilel Garcia-Pereira*, Helder R. O. Rocha**

Federal University of Espírito Santo, Vitória-ES, Brazil

**Higher School of Experimental Sciences and Technology, University of Rey Juan Carlos, Madrid, Spain*

***Federal Institute of Espírito Santo, São Mateus-ES, Brazil*

Abstract

The growing interest for researches that focus on renewable energies, as well as the increase in funding for this sector, is thanks to the advantages of renewable energy namely the reduction of environmental impacts and their great reliability. However, to maintain the correct operation of the electrical grid and its quality, it is essential to study the impacts that these generating sources have on the electrical system. The present research paper presents a novel methodology that considers the optimal allocation of photovoltaic distributed generation, capacitor bank, and fault current limiters reactors in distribution feeders, whose purpose is minimizing simultaneous the short-circuit current, active losses and harmonic distortion rate of distribution feeders. For this, a Multi-objective Gray Wolf Optimize has been applied and tested in three different distribution feeders. The result demonstrated that during the entire optimization process, the greatest reduction of the analyzed parameters, which are losses, harmonic distortion rate and short circuit current are associated with the location and number of devices that are allocated in the system.

Keywords: Distributed Generation, Capacitor Banks, Fault Current Limiters Allocations, Reducing Losses, Short-circuit, Harmonics Optimizations.

1. Introduction

Due to the growing demand for energy and greenhouse gas emissions, countries around the world are implementing targets to reduce pollutants, through improved energy efficiency and increased production of clean energy [1]. It is important to highlight the increase in the implementation of distributed generation (DG) technologies, which provide energy efficiently and are dispersed throughout the system. DG can provide several advantages to the electrical system, such as reducing power loss due to the proximity between load and generation, improving power quality, reducing voltage drop, improving the voltage profile and increasing the reliability of the power system [2].

In addition, Photovoltaic (PV) energy is variable because it leans on intermittent meteorological parameters which basically are solar radiation and ambient temperature [3]. Therefore, using PV energy as power source can produce problems in the power grid related to short-circuit currents, voltage profile, reducing the power factor, loading, harmonic distortion rate and power losses [4], [5]. Aforementioned problems can arise in particular in the case of bidirectional plants namely distributed grids (DGs), in which there exists interchange of power between the energy sources. This possibility may have significant implications in terms of electrical grid voltage and frequency while compromising the protection system reliability which is not configured for this type of scenario. Moreover, the problem may be worse since the penetration of active power affects the grid voltage by rising it, while reactive power consumption can cause voltage drops. Therefore, the use of larger DG units should be accompanied by an adequate voltage and frequency control to ensure that maximum and minimum service voltage and frequency limits are met [6], [7].

The integration of the DGs in the electrical grid can also affect the protection devices since they may generate variation in the feeders fault currents, which implies the operation variation of the over current relays, causing them to operate differently and compromising the reliability and selectivity of the protection system [8].

Moreover, the insertion of DGs may increase harmonic distortion that lead to higher temperatures in neutral conductors and distribution transformers. This is considered harmful for electrical devices since it reduces their lifespan

and damages the power grid [9].

In addition to the study of the effects of the DGs on the grid voltage and frequency and harmonics distortion, it is also important to analyze the behavior of the power system equipped with capacitors banks (CBs) and fault current limiters (FCLs). In fact, the use of CBs in distribution system is relevant to reduce power losses, ensure voltage stability and relocate some of the power system capacity. Hence, it is important to highlight the relevance of choosing properly the number and the location of CBs in the electrical grid [10].

By the same token, the design of power systems should take into account the short circuit cases and therefore cope with these cases and operate safely [11]. As it has previously been discussed, since PV plants generate variable electrical power, short-circuit current can rapidly exceed safe levels. Consequently, the use of limit fault current is crucial.

Thus, to mitigate the possible problems that may occur by the use of DGs, this research paper studies a proposal for the simultaneous optimal allocation of capacitor banks and fault current limiters in the electrical grid equipped with PV plants. The aim is to minimize simultaneously the short-circuit current, active losses and harmonic distortion rate of distribution feeders.

1.1. Related Works

In general, there are research works that studied the allocation of the DGs and the use of the aforementioned devices in the electrical grid, but separately. For example, in Al-Ammar *et al.* [10], the paper dealt with the allocation of CBs in the electrical grid of 15 and 33 nodes of the IEEE using the multi-objective optimization using the bee screening algorithm. Moreover, the research work carried out by Rahiminejad *et al.* [12] focused on the allocation of DGs and CBs, as well as the reconfiguration of distribution grids to minimize the active power losses and maximize the electrical grid reliability. However, regarding the optimization based on the cost reduction, the research work presented by Ouali and Cherkaoui [13] proposed a new methodology for the optimal investment in DG, based on the optimal allocation of DGs and CBs to alleviate the constraints of the grid voltage and reduce the cost of interconnecting renewable sources in medium voltage grids.

In Bayat and Bagheri [14], the authors proposed a new and simplified heuristic method for optimal allocation of DGs and CBs. The obtained results show that the approach presents optimal solution in a short time, in

addition to the possibility to apply it to large distribution plants. Moreover, in Ouali *et al.* [15] and Augusto *et al.* [16] optimization is used to minimize the system reconfiguration costs. Shaheen and El-Sehiemy [17] used the improved gray wolf algorithm to allocate DGs, CBs and voltage regulators with the aim to minimize the costs of coordinated equipments, maximizing the benefits arising from reduced energy losses and energy purchase. In addition, Venkatesan *et al.* [18] used a hybrid optimizer for optimal placement and sizing of DGs and CBs. Indeed, the proposed hybrid method has a high speed of convergence fulfilling an enhancement in the results in the different conflicting objectives.

A coordinated allocation methodology of DGs considering their uncertainties, CBs and soft open points in distribution networks using the bi-level programming model is presented in Zhang *et al.* [19]. The allocated equipment helped reduce energy losses and improve voltage profiles. In Quadri *et al.* [20] a comprehensive teaching learning-based optimization is presented for the optimal allocation of DGs in radial distribution systems to improve network loss reduction, voltage profile, and annual energy savings. Single and multi-objective formulations are considered and simulated in three IEEE test networks. Mouwafi *et al.* [21] presents a two-stage procedure to determine the optimal sizes and locations of GDs and CBs considering single-objective and multi-objective functions. In stage-1 it selects candidate bars and in stage 2 it uses the chaotic bat algorithm to find the sizes and locations of DGs and CBs. The results show the superiority of the proposed procedure to reduce the real total power loss and improve the voltage profile concerning the literature.

In Naderipour *et al.* [22], the authors studied the allocation of CBs in a microgrid with DG and different load levels. In fact, in this paper, the objective function included minimizing the cost of energy losses, peak power losses and the cost of capacitors. Indeed, the algorithm used allowed the losses to be reduced and the voltage profile to be enhanced during injection and non-injection of reactive power. In addition, in Pereira *et al.* [23], Genetic Algorithm (GA) is used for the optimal positioning of DGs and CBs based on technical and economic parameters. In order to preserve the horoseasonal and stochastic nature of the wind and solar energy dependency, the methodology applied used a model that involves the sequential Monte Carlo method and the diagonal band Copula model. Indeed, the algorithm demonstrated a reduction of up to 73.4% in the analyzed feeders, with adequate voltage levels and a return on investment of 7 years.

In Hamidi and Chabanloo [24], the paper focused on allocating and sizing fault current limiters using the GA to reduce losses and the negative impacts of DGs. The proposed method was implemented in two test grids and the obtained results demonstrated the efficiency of the method used. Additionally, Mahmoudian, Niasati and Khanesar [25] determined the optimal number and allocation of FCLs to improve the power grid reliability and fault current reduction. The IEEE 39 and IEEE 57 Bus system were considered to evaluate the effectiveness and feasibility of the proposed method. However, El-Ela *et al.* [26] studied the possibility of the optimal allocation of different types of DGs units correlated with FCLs to minimize the power losses, reduce the fault currents in the grid with size savings of the installed FCLs. The proposed methodology is studied in 3 systems and acceptable power losses and failure level reduction are achieved for both normal and faulty operating conditions.

1.2. Contributions

Given the aforementioned state of the art, it is possible to verify that there is no available studies that include the allocation of DGs, CBs and FCLs simultaneously intending to minimize losses, harmonic distortion and short-circuit current. Thus, this research paper presents a novel methodology whose purpose is allocating the optimal number and place of DGs, CBs and FCLs using the Multi-objective Grey Wolf Optimizer (MOGWO). After the optimization procedures, the distribution network operator can choose, through the Pareto curve, the most appropriate operating configuration for the feeder, i.e, the application of this new approach can improve the planning and operation of the electrical system performance, which is verified by the validated simulation of three study case using IEEE grid test. A preliminary study has been performed by some authors of this paper [27]. Figure 1 shows the system description adopted in this paper.

The methodology developed in the paper is performed as follow: first, *software* OpenDSS is used to model the electrical grid and MATLAB to apply the optimization of the system. Then, during the simulation process, some grid changes are applied using MATLAB. Then, the corresponding results are simulated in OpenDSS with the purpose of quantitatively identify the impacts of the aforementioned devices (DGs, CBs and FCLs) on generating losses, harmonic distortion rate and short-circuit current.

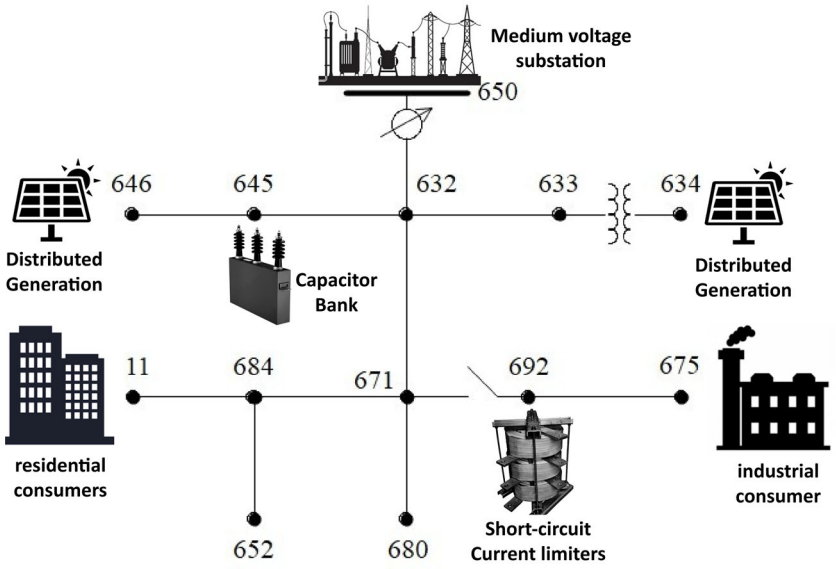

Figure 1: Example of the IEEE 13 bus system with PVs, CBs and FCLs installed.

1.3. Article Structure

This paper is structured in 6 sections. First, section 1 presents the introduction, the related work, and the research contributions. In section 2, the theoretical foundation of the topic discussed in this article is set out. Then, sections 3 and 4 present the methodology and define key parameters for modeling and simulation of the studied systems, in addition to the problem formulation and the optimization model used. The results of the performed simulations and the corresponding discussions are presented in section 5. Finally, the conclusions of the work are presented in section 6.

2. Theoretical Foundation

This section studies the theoretical foundation, highlighting the impact of DG, CBs and FCLs insertion on the electrical power system.

2.1. Impacts of the Distributed Generation

DG can be implemented with renewable and non-renewable generation. Moreover, it can be connected to the grid or operate autonomously. In fact,

the introduction of DG into the distribution system can significantly affect the power flow of the electrical grid, which can be both positive or negative, depending on the operational characteristics of the distribution system and the characteristics of DG [28]. The following aspects can be highlighted: the system capacity, the power quality, the protection, the voltage regulation, the losses, and the short-circuit current.

With the insertion of DG in the system, the amount of the power that travels through cables, power lines and transformers in the network increases. However, transformers suffer the most from this increase in the power capacity of the system [29] since that the power flow becomes bidirectional. In these new working conditions, the transformer is strained due to the reverse power flow.

In terms of the power quality, the insertion of DG can negatively affect the power system since frequency is one of the most important and sensitive parameters related with the power quality. Moreover, since there is a strong dependency between power and frequency, the installation and connection of DG to the grid will directly affect the frequency of the power system. In addition, DG can be a source of harmonics in the grid which can be either from the generation unit itself, the power electronics devices, or other equipment [30].

Nowadays, distribution grids are equipped with protection devices which purpose is to eliminate faults whenever they occur. However, as it has previously been discussed, the insertion of DG units increases the possibility of having problems related with fault currents, which can be worse due to bidirectional power flows in distribution grids and can be rose, compared to normal conditions without DG [30]. Hence, the operation of the protection devices should be coordinated, which means that DGs should be synchronized with the grid operation [31] and recloser should be selected based on the DG size, type and location [32].

The system efficiency is affected by the electrical line resistance. Besides, it depends on the electrical grid topology and the loading rate [33]. In addition, DG location and capacity affects the system efficiency since when DG is inserted into a distribution grid, this increases the power flow near to load, which may reduce losses locally. Thus, the exceeded power is injected in the electrical grid whenever is needed. The variation of the active power ΔP_k at bus k is defined by the following Eq. 1.

$$\Delta P_k = P_{Dk} - DG_k \times P_{DGk} \tag{1}$$

where P_{Dk} is the active power (W) required at bus k, DG_k is the binary variable to determine the presence of DG at bus k, P_{DGk} is the active power (W) inserted by DG at bus k.

2.2. Capacitor Bank in the Electric Power System

In electrical power systems, CBs are used to enhance the reactive power when they are connected in parallel to the load, in such a way that the power factor is corrected and losses in the lines are decreased. However, the connection in series is to conserve the voltage at a certain level. Eq. 2 describes the variation of the reactive power ΔQ_k ($kvar$) inserted at the bus k:

$$\Delta Q_k = Q_{Dk} - CB_k \times Q_{CBk} \tag{2}$$

where Q_{Dk} is the reactive power ($kvar$) demanded at bus k, CB_k is the binary variable to determine the presence of CB at bus k and Q_{CBk} is the reactive power ($kvar$) injected by CB at bus k.

2.3. Fault Current Limiters in the Electric Power System

The purpose of using FCLs is to control the short-circuit currents levels in the cases that they exceed the nominal levels tolerated by the electrical grid [24]. To do so, FCLs should fulfill the following requirements: small impedance in normal operating conditions, high impedance during short-circuit currents cases, rapid elimination of faults with the capacity of fast returning to the normal operating of the grid. In addition, it is important that FLCs have good reliability during prolonged duration joined with maintaining the good quality of the plant operation, which also means less costs for maintenance [25], [26].

In this research paper, air-core FCLs are used thanks to their good reliability when reducing short-circuit current, in addition to the existence of this type of devices with important operation intervals. Eqs. 3, 4 and 5 describe the calculation of the corresponding RLC impedance Z_{RLC}.

$$Z_{RLC} = (\frac{1}{q} \ + \ j) * X_{RLC} \tag{3}$$

$$X_{RLC} = \frac{Q_{RLC}}{V_{RLC}^2} \tag{4}$$

$$q = \frac{X_{RLC}}{R_{RLC}} \tag{5}$$

where X_{RLC} is the reactance of the FCL, R_{RLC} is its resistance, Q_{RLC} corresponds to its rated power, V_{RLC} is its rated voltage and q corresponds to its quality factor.

3. Allocation Methodology of DGs, CBs and FCLs

To quantitatively analyze the impacts that DGs, CBs and FCLs can cause on the system losses, harmonic distortion rate and short-circuit current, a Multi-Objective Grey Wolf Optimizer (MOGWO) implemented in MATLAB is used in conjunction with OpenDSS software to analyze the IEEE 13, 34 and 123-node feeders. The developed methodology uses the OpenDSS software to model the network and perform the power flow, curt-circuit, and harmonic analyses, while MATLAB applies the system optimization. During the simulation process, network changes are made in MATLAB and each change is simulated in OpenDSS.

3.1. Validation of IEEE networks

Before performing the optimization step, first the validation step is carried out by calculating the percentage error between phase voltages and the lines current values of the modeled network which were obtained by solving the power flow problem using OpenDSS, and the values of these parameters in the IEEE report. Once the validation is effectuated, the power system can undergo the necessary changes to perform the optimization.

3.2. OpenDSS Usage Methodology

OpenDSS is an electrical distribution system simulator software that operates in the frequency domain, in which voltages and currents are in sinusoidal steady state.

3.2.1. Distributed Generation

The Photovoltaic Panel model is an aggregated model of a solar panel model together with an inverter that is able to quickly find the maximum power point of the panel (MPP).

According to [34], the program execution process in the presence of the photovoltaic panel is divided into six steps, which are described below:

Step 1 - Calculation of the output power of the photovoltaic panel: The output power, $P_{DC}(t)$, of the panel is calculated according to Eq. 6.

$$P_{DC}(t) = P_{mpp} \times irrad \times irradiance(t) \times PT_{Curve}[Temp(t)] \tag{6}$$

where: t is the time interval, $irrad$ is the base value of the radiance per kW/m^2, $irradiance(t)$ is the value of the irradiance curve in the time interval t, $PT_{Curve}[Temp(t)]$ is the value of the correction factor in the time interval t due to temperature.

Step 2 - Inverter state check: The inverter state at the time instant t depends on its state at the previous time instant, $t-1$. Therefore, Eq. 7 changes the inverter state to ON when the state at $P_{DC}(t-1) = 0$ is OFF.

$$Status(t) = ON, \, if \, P_{DC} \geq \frac{\%cutin \times kVA}{100} \tag{7}$$

where $\%cutin$ is a percentage of the inverter's nominal power, $Status(t)$ indicates whether the inverter is on or off, kVA is the inverter's power in kVA.

Therefore, Eq. 8 switches the inverter state to OFF when the state at $P_{ac}[t-1] > 0$ is ON.

$$Status(t) = OFF, \, if \, P_{DC} < \frac{\%cutin \times kVA}{100} \tag{8}$$

Step 3 - Calculation of the active power required by the inverter: The desired active output power of the inverter, $P'_{ac}(t)$, is calculated using Eq. 9. In this step, the maximum active power limit is also verified through the property $Pmpp$ of the photovoltaic panel and the active power limit, $P_{Lim}(t)$, which results from an eventual operation of the volt-watt function of an InvControl (C_{vw}) element that can control the panel.

$$P'_{ac}(t) = \begin{cases} 0,\ Status(t)\ =\ OFF \\ P_{LimMin}(t),\ if\ P_{DC}(t) \times EFF \geq P_{LimMin}(t) \\ P_{DC}(t) \times EFF \end{cases} \tag{9}$$

$$P_{LimMin}(t) = \begin{cases} min(\frac{\%Pmpp \times Pmpp}{100}, P_{Lim}(t)),\ P_{Lim}(t)\ ofC_{vw} \\ \frac{\%Pmpp \times Pmpp}{100} \end{cases} \tag{10}$$

where P_{LimMin} is the minimum Active Power limit and EFF is the efficiency of the inverter.

Step 4 - Calculation of the reactive power required by the inverter: The desired reactive power of the inverter, Q'_{ac}, is defined separately from the active power and can be specified as a fixed kvar value or as a function of a constant power factor. The inverter will try to keep the reactive power value constant at the kvar value that has been specified, regardless of the current value of the active power output.

Step 5 - Checking the inverter's reactive power limits: The desired reactive power after checking its limits is presented in the Eqs. 11 and 12.

$$Q"_{ac}(t) = \begin{cases} Q'_{ac}(t),\ if\ Q'_{ac} < |Q_{Limit}(t)| \\ |Q_{Limit}(t)|,\ if\ Q'_{ac}(t) \geq |Q_{Limit}(t)| \end{cases} \tag{11}$$

$$Q"_{ac}(t) = \begin{cases} -|Q_{Limit_{neg}}(t)|,\ if\ Q'_{ac} < -|Q_{Limit_{neg}}(t)| \\ |Q'_{ac}(t)|,\ if\ -|Q_{Limit_{neg}}(t)| \leq |Q'_{ac}(t)| \end{cases} \tag{12}$$

Eq. 11 is used when the desired value of the reactive power, Q'_{ac}, is positive and Eq. 12, when it is negative. Furthermore, Eq. 13 and Eq. 14 present the limits of the reactive power supplied and absorbed, respectively, as a function of the active power supplied to the grid.

$$|Q_{Limit}(t)| = \begin{cases} 0,\ if\ P_{ac} < P_{min} \\ \frac{kvarMax}{P_{max}},\ if\ P_{min} \geq P_{ac}(t) < P_{max} \\ kvarMax,\ if\ P_{ac}(t) \geq P_{max} \end{cases} \tag{13}$$

$$|Q_{Limit_{neg}}(t)| = \begin{cases} 0,\ if\ P_{ac} < P_{min} \\ \frac{kvarMaxAbs}{P_{max}},\ if\ P_{min} \geq P_{ac}(t) < P_{max} \\ kvarMaxAbs,\ if\ P_{ac}(t) \geq P_{max} \end{cases} \tag{14}$$

Step 6 - Inverter capacity check: The maximum inverter capacity corresponds to its power rating in kVA. Active and reactive power that are supplied to the grid can be defined, $P_{ac}(t) = P'_{ac}(t)$ and $Q_{ac}(t) = Q"_{ac}(t)$, respectively. If the maximum capacity of the inverter is exceeded, the inverter limits the value of $|\bar{S}(t)|$ to the maximum power value defined by the user in the variable kVA. Therefore, the values of $P'_{ac}(t)$ and/or $Q"_{ac}(t)$ must be reduced to meet one of the following three priorities: power factor priority, active power priority and reactive power priority.

The Eqs. 15 and 16 present the active and reactive power values that the inverter must supply to the grid when the inverter capacity is exceeded in the case of power factor (PF) priority.

$$P_{ac}(t) = kVA \times |PF| \tag{15}$$

$$Q_{ac}(t) = kVA \times \sqrt{1 - PF^2} \times Signal(PF) \tag{16}$$

Eq. 17 presents the new reduced reactive power value that is delivered to the circuit when the inverter capacity is exceeded in the case of active power priority. If the active power is greater than or equal to the inverter capacity, the new active power value that is delivered to the grid becomes the kVA rating and, therefore, the reactive power becomes null, according to Eq. 18.

$$Q_{ac}(t) = \sqrt{kVA^2 - P_{ac}(t)^2} \tag{17}$$

$$P_{ac}(t) = \begin{cases} kVA, \ if \ P'_{ac}(t) \geq kVA \\ P'_{ac}(t) \end{cases} \tag{18}$$

Eq. 19 presents the new reduced active power value that is delivered to the circuit when the inverter capacity is exceeded. If the reactive power is greater than or equal to the inverter capacity, the new value of the reactive power becomes the capacity of the inverter itself, according to Eq. 20, but this can only happen if the inverter is capable of providing or absorbing reactive power without any active power.

$$P_{ac}(t) = \sqrt{kVA^2 - Q_{ac}(t)^2} \tag{19}$$

$$Q_{ac}(t) = \begin{cases} kVA \times Signal(Q"_{ac}(t)), \ if \ |Q"_{ac}(t)| \geq kVA \\ Q"_{ac}(t) \end{cases} \tag{20}$$

Finally, the apparent power supplied by the photovoltaic panel at an instant t can be written according to Eq. 21.

$$\bar{S(t)} = P_{ac}(t) + jQ_{ac}(t) \tag{21}$$

Figure 2 illustrates the irradiation curve used to model the photovoltaic panel for the 24-hour interval. It can be seen in Figure 2 that the highest irradiation is found at 12 hours. The irradiation has a null value in the time interval between 0 and 6 hours and after the 20 hour mark. During fault mode simulation, the most critical case for three-phase and single-phase faults are always analyzed.

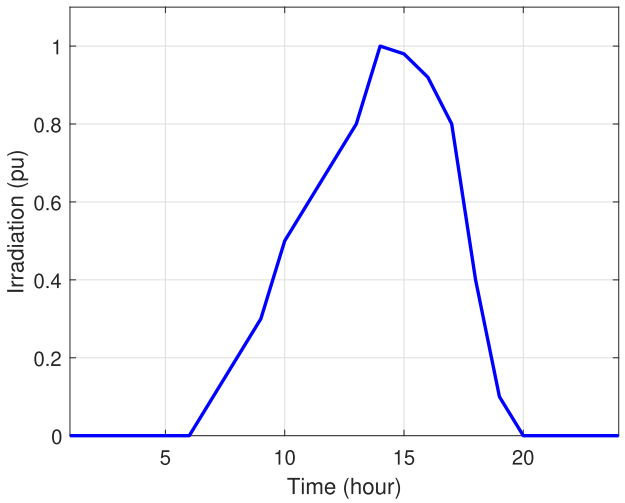

Figure 2: Daily Irradiation Curve used in the methodology

3.2.2. Power Flow

The Power Flow solution method in OpenDSS works directly from the system's nodal admittance matrix, that is, using the system's nodal voltages and injected currents phasors. The elements available in the software are categorized into three groups: control element, power delivery element (PD) and power conversion element (PC) [35] and to find the power flow solution,

the method uses an iterative fixed-point algorithm, as decribed in four steps below.

Step 1 - Initial step: It consists of performing a direct solution of the nodal admittance matrix, $\bar{Y}_{system}$, considering that the compensation current is null for all PC elements.

Step 2 - Calculation of compensation currents for each PC element: OpenDSS calculates the compensation current injected by each PC element and stores all injected currents in the vector $\dot{I}_{inj}$.

Step 3 - Solution for a new vector of nodal voltages: With the updated vector of injected currents, a new solution of the system: $\dot{V}_{nodal} = [\bar{Y}_{system}]^{-1} \times \dot{I}_{inj}$ is calculated using $KLUSolve$, which is the solver used by OpenDSS.

Step 4 - Convergence test: In this step, the convergence of the system to a solution is checked. If convergence is reached, the iterative process ends at this step. Otherwise, the system returns to steps two and three until convergence or until the maximum number of iterations is reached. In the default configuration, the Power Flow Solving Algorithm converges when $error_i < 0.0001 \ \forall \ i$.

Figure 3 illustrates the load curve profile that will be used to model the daily behavior of the network.

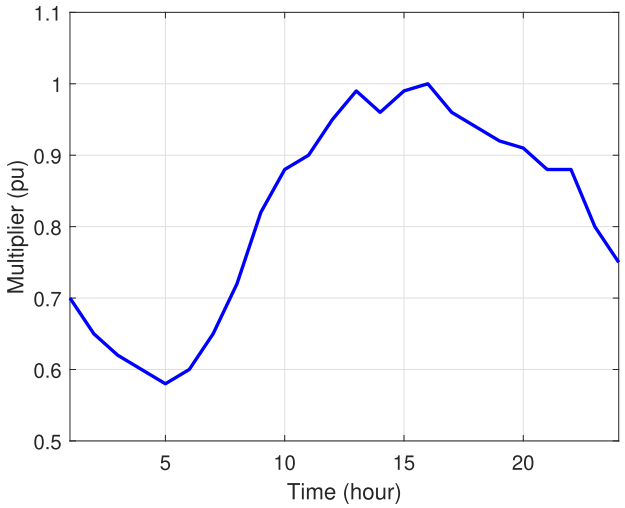

Figure 3: Load curve multiplier for daily simulation

The network behavior in the 24 hours time frame was used as input in the

optimization of the losses and the harmonic distortion rate. In this study, the impacts of the harmonic distortion rate on distributed loads will not be analyzed, since loads have been considered, mathematically, as concentrated loads grouped in a certain location of the power system. In addition, the allocation of DGs, CBs and FCLs can only take place on the fixed nodes of the network.

3.2.3. Harmonics

According to [35], in harmonic analysis the user can define several harmonic spectra to represent harmonic sources of interest. In addition, the software has several spectrum standards already defined. After spectrum definition, harmonic sources can be connected to load, generator, voltage source, current, and other power conversion elements as desired. The program starts by running an instantaneous power flow to initialize the problem. After that step, the harmonic sources are then initialized to the appropriate magnitudes and phase angles for each solution.

OpenDSS allows the use of two commands for harmonic analysis: Harmonics, which is the most suitable method when there is no time and control action involved, and HarmonicT, which defines the harmonic solution mode with time and control actions involved.

It is worth mentioning that in both commands there must be a successful power flow solution so that the rotatory machines and harmonic sources can be started. The processes of the two modes are similar, the loads are converted into harmonic current sources and initialized based on the power flow solution according to the *Spectrum* multiplier. Generators are converted into a voltage source through their subtransient reactance with the voltage spectrum specified for each generator. Finally, the matrix Y_{system} is constructed for each frequency and solved with injections from all harmonic sources following Eq. 22.

$$I_h = Y_{system} \times V_h \tag{22}$$

where: I_h is the phase current a,b,c for the harmonic h and V_h is the phase voltage at each node for the harmonic h. The THD calculations are defined by the Eqs. 23.

$$THD = \frac{I_H}{I_F} = \frac{\sqrt{\sum_{h=2}^{n} {I_h}^2}}{I_F} \tag{23}$$

where: I_H is the total harmonic current by phase, I_F is the fundamental harmonic component of the current and I_h^{abc} the h-th harmonic component of the current.

3.2.4. Short Circuit

OpenDSS describes the power system by constructing its nodal admittance matrix. The study of short-circuit current can occur through two methods [36]: *Fault Simulation* which consists of a simulation of a specific fault determined by the location and definition of one or more fault objects in the feeder and *Fault Study* which consists of a general study of the faults in the feeder.

The simulation of a specific fault allows the application of different types of faults (single-phase, two-phase and three-phase, among others). Fault simulation in *Fault Simulation* mode consists of applying a resistor that can have its resistance value determined between the desired phase and the fault point. This type of simulation also allows the application of several faults simultaneously, which allows a more accurate study of the fault points.

In the *Fault Study* mode, the program builds a nodal admittance model (Y matrix) of the system. The voltage sources are converted to Norton equivalents and the resulting admittance is incorporated into the system Y matrix. After building the nodal admittance model, OpenDSS solves the Eq. 24 for the phase voltages of each node:

$$I_{inj} = Y_{system} \times V_o \tag{24}$$

where I_{inj} is the injected current and V_o is the phase voltage at each node.

The fault study of the mode in question is based on a polyphase Thevenin equivalent on each bus. The first step of this method is based on the calculation of the open circuit voltage vector on each bus. This is done by running a direct solution immediately after starting the *Fault Study* mode.

Since the matrix Y_{system} already assumes that the voltage sources are shorted, the short-circuit matrix is determined by injecting a current of 1 +

j0 A into each bus node. Then, the short-circuit matrix, Z_{sc} represented in Eq. 25, is calculated for each bus, as shown in Eq. 26.

$$Z_{sc} = \begin{bmatrix} Z_{11} & Z_{12} & Z_{13} \\ Z_{21} & Z_{21} & Z_{23} \\ Z_{31} & Z_{32} & Z_{33} \end{bmatrix} \tag{25}$$

$$Y_{sc} = Z_{sc}^{-1} \tag{26}$$

The short-circuit currents, I_{sc}, are now calculated according to Eq. 27.

$$I_{sc} = Y_{sc} \times V_{sc} \tag{27}$$

Eq. 27 represents the fault current of all phases of OpenDSS. These currents are the short-circuit currents that would flow from each node if all nodes on the bus were shorted to node 0, which represents the ground node. Note that these currents will not be equal if the impedances are not balanced (or the open circuit voltages are not balanced).

Finally, it is important to note that in this solution mode OpenDSS only reports adjacent phase faults (1-2, 2-3, 3-4, etc.). It does not report failures in phases 1-3, for example. This is a peculiarity that can eventually be changed by using an interface with *MATLAB* that makes it possible to extract the matrix Z_{sc} from OpenDSS.

4. Problem Formulation and the Optimization Model Used

This section describes the formulation of the optimization problem and the Grey Wolf optimization method applied.

4.1. Problem Formulation

Optimization algorithms should include information related with the problem objectives and the corresponding decision variables from the one hand and specify the constraints and problem type, from the other one. In fact, the objective definition consists in planing the goals to be fulfilled by acting on the decision variables. Similarly, constraints defines the limits that should be respected by the variable values.

In this paper, same objective functions are used for grids with 13, 34 and 123 buses, while constraints are adapted for each type of the mentioned grid. The following relations given by Eqs. 28, 29 and 30 describe the objective functions applied for this study.

$$Min\ f_1 = \sum_{i=1}^{24} Loss_i \tag{28}$$

$$Min\ f_2 = mean(\sum_{j=1}^{n} THD_j) \tag{29}$$

$$Min\ f_3 = mean(\sum_{k=1}^{n} TriFault_k + \sum_{k=1}^{n} SingFault_k) \tag{30}$$

where $Loss_i$ are the total active power losses for each time interval i in hours, used to calculate f_1 which is the sum of the daily losses. THD_j corresponds to the harmonic distortion rate of the feeder node $j-th$, used to evaluate f_2 which is the averages of the harmonic distortion rate. n corresponds to the number of the studied nodes network. $TriFault_k$ and $SingFault_k$ are the three-phase and single-phase fault current, respectively at node $k-th$.

Constraints that correspond to each network type are described by Eqs. 31, 32 and 33.

$$n_{CB13} \leq 6, n_{FCL13} \leq 6, n_{DG13} \leq 6 \tag{31}$$

$$n_{CB34} \leq 16, n_{FCL34} \leq 16, n_{DG34} \leq 16 \tag{32}$$

$$n_{CB123} \leq 63, n_{FCL123} \leq 63, n_{DG123} \leq 63 \tag{33}$$

where n_{CBx} correspond to the number of CBs, n_{FCLx} is the number of FCLs, n_{DGD} is the number of DGs used in the grid composed of x nodes. Such maximum values (6, 16 and 63) are large enough not to reduce the search space of the algorithm, whose values were defined after an exhaustive analysis search was performed with multiple simulations.

The power flow and voltage limits are expressed using Eqs. 34, 35 and 36.

$$\sum_{i=1}^{n} P_i^{sp} - \sum_{i=1}^{n} P_i^{calc} = 0 \tag{34}$$

$$\sum_{i=1}^{n} Q_i^{sp} - \sum_{i=1}^{n} Q_i^{calc} = 0 \tag{35}$$

$$V_i^{min} \leq V_i \leq V_i^{max} \quad \forall_i \ \epsilon \ \Omega_n \tag{36}$$

where n are the grid buses, P_{sp} is the specified active power, P_{calc} is the calculated active power, Q_{sp} is the specified reactive power, Q_{calc} is the calculated reactive power, all of them are provided to OpenDSS, V_i is the voltage at the system bus, V_i^{min} is the minimum voltage limit, V_i^{max} is the maximum voltage limit and Ω_n is the system bus.

4.2. Pareto Curve in Multi-Objective Optimization

Pareto optimization is a key concept in multi-objective optimization problems that is grounded on that they cannot be enhanced at the same time [37]. In fact, [37] defines Pareto optimization as the minimization of the n components of f_k, with $k = 1, ..., n$, of a vector function f of a vector variable x in a universe U, where $f(x) = (f_1(x), ..., f_n(x))$. Indeed, the decision vector $x_u \ \epsilon \ U$ is Pareto optimal whenever there is no $x_v \ \epsilon \ U$ such that $v = f(x_v) = (v_1, ..., v_n)$ dominate $u = f(x_u) = (u_1, ..., u_n)$. Thus, there is no $x_v \ \epsilon \ U$ so that: $\forall \ i \ \epsilon \ \{1, .., n\}, \ v_i \leq u_i \quad \& \quad \exists \ i \ \epsilon \ \{1, .., n\}, \ v_i < u_i$. Hence, the set of vectors that fulfill this condition is called the Pareto-optimal set. Moreover, the corresponding set of objective vectors is called the non-dominated set.

4.3. Multi-Objective Gray Wolf Optimizer

Gray wolf optimization algorithm is an optimization technique that is inspired by the hierarchy and the hunting strategy of gray wolves. According to this algorithm, the pack of wolves represents the optimizer and the prey is considered the solution [38]. Alpha wolf (α) is the leader of the group while the second and third leaders are beta (β) and delta (δ) respectively, asked to assist the other wolves and contribute during decision making of wolf (α). As the organization of wolves pack is hierarchical, omega (ω) wolves are those characterized by with the lowest ranking in the group. In addition, when searching for the solution that optimizes the problem, Gray wolf optimization algorithm adopts the same manner of wolves group when hunting. Indeed, during the hunting stage, wolves surround the prey. This is exactly is applied

by the Gray wolf optimization algorithm and is mathematically described by the Eqs. 37 and 38.

$$\vec{D} = |\vec{C} \cdot \vec{X}_p(t) - \vec{X}(t)| \tag{37}$$

$$\vec{X}(t+1) = \vec{X}_p(t) - \vec{A} \cdot \vec{D} \tag{38}$$

where t indicates the iteration, $\vec{A}$, $\vec{C}$ and $\vec{D}$ are coefficient vectors, $\vec{X}_p$ is the position vector of the prey and $\vec{X}$ indicates the position vector of gray wolves. Vectors $\vec{A}$ and $\vec{C}$ are calculated according to the Eqs. 39 and 40.

$$\vec{A} = 2\vec{a} \cdot \vec{r_1} - \vec{a} \tag{39}$$

$$\vec{C} = 2 \cdot \vec{r_2} \tag{40}$$

The components of $\vec{a}$ decrease linearly from 2 to 0 with iterations, and $\vec{r_1}$ and $\vec{r_2}$ are random vectors ranging from 0 to 1. The Eqs. 39 and 40 allow the position of the wolves to be updated according to the position of the prey. Random value vectors, $\vec{r_1}$ and $\vec{r_2}$, allow wolves to be placed in different positions to encircle prey. The hunting stage is led by the α wolf and the β and δ wolves. The proposed mathematical model obeys Eqs. 41, 42 and 43.

$$\vec{D_\alpha} = |\vec{C_1} \cdot \vec{X_\alpha} - \vec{X}|, \vec{D_\beta} = |\vec{C_2} \cdot \vec{X_\beta} - \vec{X}|, \vec{D_\delta} = |\vec{C_3} \cdot \vec{X_\delta} - \vec{X}| \tag{41}$$

$$\vec{X_1} = \vec{X_\alpha} - \vec{A_1} \cdot (\vec{D_\alpha}), \vec{X_2} = \vec{X_\beta} - \vec{A_2} \cdot (\vec{D_\beta}), \vec{X_3} = \vec{X_\delta} - \vec{A_3} \cdot (\vec{D_\delta}) \tag{42}$$

$$\vec{X}(t+1) = \frac{\vec{X_1} + \vec{X_2} + \vec{X_3}}{3} \tag{43}$$

The idea here is that the wolf makes attack to the prey when this stops moving. Indeed, this behavior is mathematically modeled by reducing the value of $\vec{a}$. In addition, gray wolves search for prey based on the position of the α, β and δ wolves, since they are the wolves with the most importance in the pack. In order to mathematically model diversity, the vector $\vec{A}$ is defined

with random values greater than 1 or less than -1, to have global search space and avoid local solutions.

According to [39], to integrate multi-objective optimization in GWO it was necessary to include two new components in the optimization process. The first component is a file that has the function of storing non-dominant Pareto-optimal solutions. The second component consists of a leader selection engine that assists in choosing alpha, beta and delta solutions.

In multi-objective optimization, solutions cannot be easily compared due to Pareto optimal concepts. However, the leader selection mechanism is designed to deal with this problem. As described above, there is an archive of the best non-dominated solutions that were obtained, so the leader selection engine chooses the least congested segments of the search space and offers one of its non-dominated solutions as alpha, beta, or delta wolves. The Algorithm 1 explains in detail the step-by-step optimization process of MOGWO.

Algorithm 1 *Multi-Objective Gray Wolves Optimizer (MOGWO)*

Initialize the wolf population X_i (i = 1,2,...,population size)
Initialize vectors a, A and C
Calculation of the objective function value for each agent
Search for non-dominated solutions and update the file with them
X_α = leader selection in the file
Exclude α from file, to avoid selecting the same leader
X_β = leader selection in the file
Exclude β from file, to avoid selecting the same leader
X_δ = leader selection in the file
Add back the α and β in the file
$t = 1$;
while $t <$ Maximum number of iterations **do**
  for i $\leftarrow$ 1 **to** population size **do**
  Update the position of each search agent
  end for
  Update vectors a, A and C
  Calculation of the objective function value for each agent
  Find the non-dominated solutions
  Updates the file with the non-dominated solutions found
  if file is full **then**
    Reorganize the file to add the new solution
  end if
  if non-dominated solutions are out of file **then**
    update the file to add the new solutions
  end if
  X_α = leader selection in the file
  Exclude α from file, to avoid selecting the same leader
  X_β = leader selection in the file
  Exclude β from file, to avoid selecting the same leader
  X_δ = leader selection in the file
  Add back the α and β in the file
  $t = t + 1$
end while
return the file =0

To carry out the optimization using MOGWO, it is necessary to pre-

viously define the population size and the maximum number of iterations. Therefore, a population of 100 wolves has been used with a maximum number of 400 iterations for networks of 13, 34 and 123 nodes. MOGWO was chosen because it was successfully implemented in other [40] optimization problems, which justifies its utility in this study.

4.4. Definition of Decision Variable Vectors

In this subsection, the vectors of decision variables implemented in the coding of the power system are further explained. These vectors were divided to achieve better simulation time and better algorithm efficiency.

4.4.1. DGs Vector

The Photovoltaic Panel used in the simulation was modeled to provide the corresponding power to each load that is allocated to the 13, 34 and 123 nodes. During the simulation process, the optimizer checks which panels should be activated according to the DGs vector to obtain the best result to minimize losses, short-circuit current and harmonic distortion rate.

4.4.2. CBs Vector

For the allocation of CBs, the strategy implemented chooses a power value of the CB between the values of 50, 100, 150, 200, 300, 400, 500, 600, 700 and 800 kvar, which are values defined in the [41] norm. The CBs that were previously allocated to the network before optimization are kept throughout the optimization process.

4.4.3. FCLs Vector

The strategy used for the allocation of FCLs chooses the value of the impedance of the reactor between the values of 5, 10, 12, 15, 18, 20, 25 and 30 ohms. The optimizer selects one of the possible values of impedance for the RLC and allocates it in the system in order to obtain a better result for minimizing losses, short-circuit current and harmonic distortion rate.

4.4.4. Network Nodes Vector

The vectors relative to the nodes of the IEEE 13, 34 and 123 nodes were separated into 3 groups: three-phase, two-phase and single-phase. The 34-node network only has three-phase and single-phase nodes, whereas networks with 13 and 123 nodes have three-phase, two-phase and single-phase nodes.

5. Results

In this section, the results of the validation of each simulated network are presented. Following the validation results, the results from the optimization process with MOGWO are presented and discussed. Two points have been chosen at the extremes of the Pareto curve generated by the MOGWO and a point near the knee of this same curve, to show the impacts of the amounts of DGs, CBs and FCLs that are allocated based on Pareto solutions. Furthermore, the values of short-circuit current, losses and harmonic distortion rate of the chosen points are compared with the initial values of each feeder, before performing the optimization.

Two different hours in the available 24 hours a day range have been selected to capture the power system network state under very different working conditions. Hours chosen have been $t = 5$ and $t = 16$ (Figure 3), which represent the time of the day with lowest and highest power load, respectively. The impact of the allocation of DGs, CBs and FCLs on the network voltage profile of each point chosen on the Pareto curve at these hours is analyzed.

5.1. Validation of IEEE Feeds in OpenDSS

To carry out all the steps described in this study, it is first necessary to validate the model in the software used for the simulation. To carry out the validation, the OpenDSS software was used and the results were compared with those available in the IEEE report [42]. Table 1 details the difference between the values obtained in the IEEE report for the 13-node system and the values obtained in the simulation for the voltage values. Table 2 details the differences in current values between the report and the simulation in OpenDSS.

Table 1: Difference in Voltage values between the simulated network and the report provided by the IEEE.

Node	Phase A		Phase B		Phase C	
	Mag	Ang	Mag	Ang	Mag	Ang
650	0.01%	0.00%	0.00%	0.00%	0.00%	0.00%
632	-1.99%	0.00%	1.26%	-0.07%	1.30%	0.03%
633	0.66%	-1.56%	1.26%	-0.02%	1.31%	0.02%
634	0.69%	-2.17%	-0.51%	0.34%	-0.55%	-0.39%
645	-	-	1.28%	0.00%	1.30%	0.05%
646	-	-	1.27%	-0.02%	1.30%	0.08%
671	0.73%	-1.89%	1.20%	-0.05%	1.32%	0.02%
680	0.73%	-1.89%	1.20%	-0.05%	1.32%	0.02%
684	0.73%	-1.50%	-	-	1.33%	0.02%
611	-	-	-	-	0.56%	0.07%
652	0.73%	-0.95%	-	-	-	-
692	0.73%	-1.69%	1.20%	-0.05%	1.31%	0.02%
675	0.74%	-0.72%	1.20%	-0.07%	1.32%	0.03%

Table 2: Difference in Current values between the simulated network and the report provided by the IEEE.

2*Node	Phase A		Phase B		Phase C	
	Mag	Ang	Mag	Ang	Mag	Ang
RG-632	0,00%	0,00%	0.00%	0.00%	0.00%	0.00%
632-633	-0.70%	0.00%	-1.33%	-0.01%	-1.40%	0.10%
632-645	-	-	-0.20%	-0.17%	1.28%	-1.35%
632-671	-0.76%	-0.63%	-1..36%	-0.40%	-1.01%	0.30%
633-Transf	-	-	-1.33%	-0.01%	-1.38%	0.09%
Transf-634	-	-	-1.32%	-0.01%	-1.39%	0.09%
645-646	-	-	1.28%	-0.02%	1.28%	0.05%
671-680	0.00%	0.00%	0.00%	0.00%	0.00%	0.00%
671-684	0.59%	-0.20%	-	-	-0.01%	0.35%
671-692	-	-	-	-	-1.30%	0.63%
684-611	-	-	-	-	-	-
684-652	0.59%	-0.20%	-	-	-	-
692-675	-0.74%	-6.80%	1.58%	-1.29%	-1.50%	0.89%

In summary, it is important to highlight that the errors found for the voltage and current values can be explained due to the fact that OpenDSS

uses a different power flow calculation method than the one used in the IEEE reports. Furthermore, each type of simulation used has a maximum number of iterations and admits a specific error for convergence, which evidently produces different results.

For the 34-node feeder, it is observed that the voltage values presented similar results to the results available in the IEEE report, however, the current values, in some cases, presented a percentage difference. This difference is due to the fact that OpenDSS models the distributed loads at 2/3 of the line while in the IEEE report these loads are modeled at 1/3 of the line. The 34-node network has a greater amount of distributed loads, which justifies the increase in the percentage error in the current value at some points in the network.

In the 123-node feeder, the percentage errors presented values very close to zero, which shows that the modeling can simulate the 123-node network very close to the simulation performed in the IEEE tests. The absence of distributed loads contributed to a better percentage error of line currents compared to the 34-node network.

5.2. Optimization Results

To evaluate the performance of the proposed methodology, three case studies were conducted and their results were compared with the respective Base Case results (without optimization).

5.2.1. IEEE 13-node network (Case Study 1)

Pareto curve obtained by the application of MOGWO in IEEE 13 node network shows better performance in the knee region, which describes the most attractive operation point [43]. For the results analysis, three points are selected to be studied in depth: the first point is at the knee of Pareto curve and the two other points are situated at the end of the curve (Figure 4). Then, a comparison of these values with those obtained without performing any optimization is detailed.

Table 3 describes the enhancements in the reduction related with THD rate, active power losses and short current levels thanks to the application of MOGWO. Whereas Table 4 describes the devices number distributed at the aforementioned points on the Pareto curve.

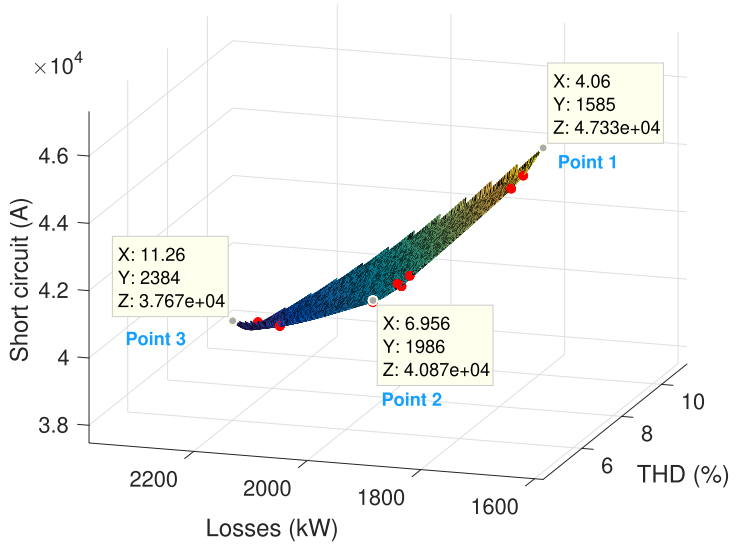

Figure 4: Optimization result in the 13-node Network with the chosen points.

Table 3: Comparison of values with and without optimization in the 13-node network

Parameters	Without Optimization (Case Base 1)	MOGWO					
		Point 1	Reduction	Point 2	Reduction	Point 3	Reduction
THD(%)	11.86	4.06	65.77%	6.95	41.40%	11.26	5.06%
Loss(kW)	2199.7	1584.76	27.96%	1986.49	9.69%	2384.19	**-8.39%**
S. circuit(A)	45262	47326.5	**-4.56%**	40865.88	9.71%	37668.5	16.78%

Table 4: Devices number distributed at each selected point of Pareto curve in the 13-node network

Devices	Point 1	Point 2	Point 3
DGs	4	2	1
CBs	2	2	2
FCLs	1	1	2

Table 3 shows that there is a raise in the short-circuit current in point 1 accompanied with losses in point 3. Therefore, as shown in Table 4, although the number of elements is similar, the places of their allocation have different consequences in term of rate of THD, active power losses and short circuit current.

The effect of using these devices in the case of three- phase fault current

in the 13-bus grid is described in Figure 5.

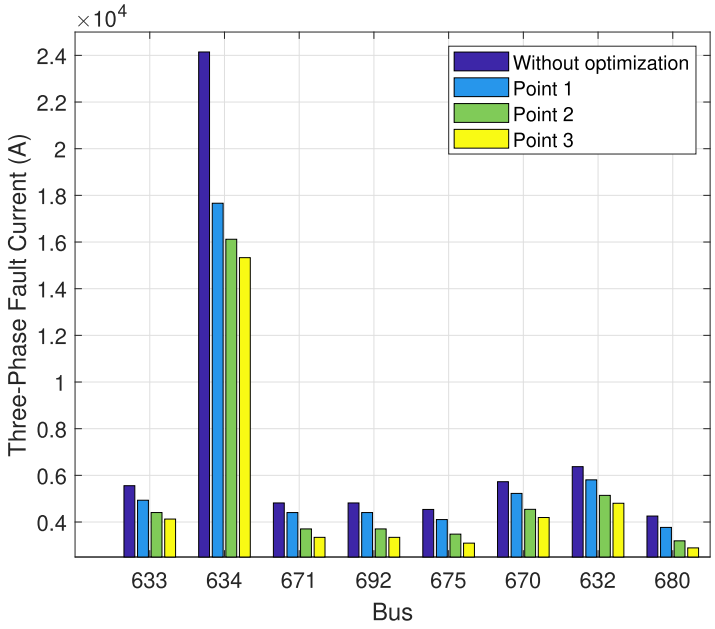

Figure 5: Three-Phase Fault Current of the 13-bus grid

The figure shows that the three-phase short circuit current is reduced in all the nodes. Moreover, node 634 has the greatest reduction in fault current compared with the other three-phase nodes of this network. This result is detailed in Figure 6 in which the active power losses in the 13-node network are represented during 24 hours.

Following the results described in this figure, the active losses reduction happens between 9 hour and 18 hour for points 1 and 2. However, point 3 faces an increment in these losses since the FCLs number is higher and the photovoltaic DGs allocated are less than in the other points.

Figure 7 describes the average harmonic distortion rate during 24 hours.

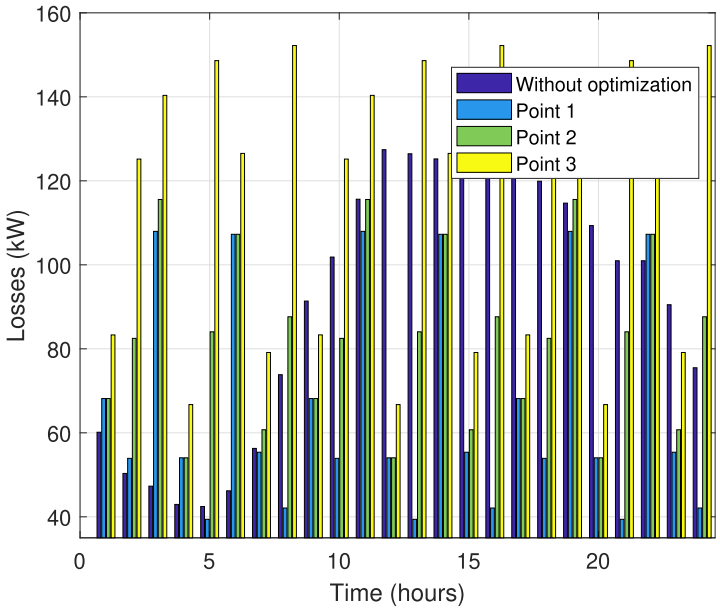

Figure 6: Daily active power losses in the 13 IEEE node Network

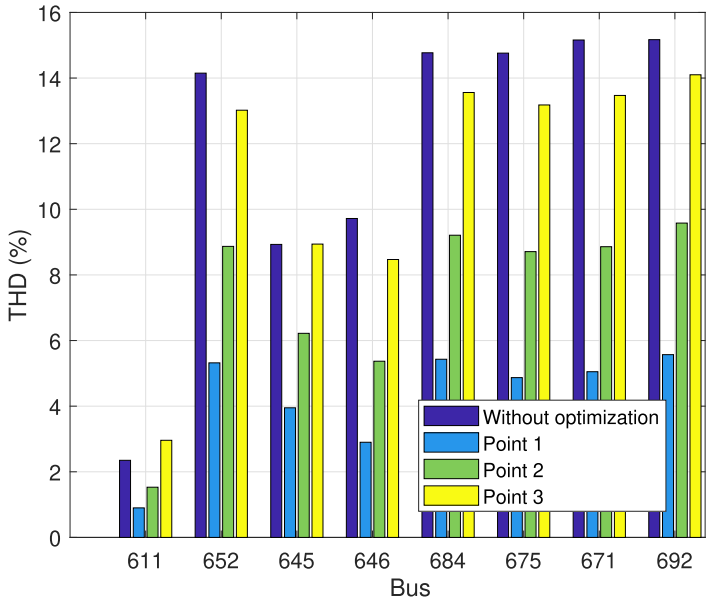

Figure 7: Average Network Harmonic Distortion Rate in the 13 IEEE node grid

The results show that the harmonic distortion rate are reduced in the three analyzed points in this case of grid. Exceptionally point 3 faced an increase in the harmonics rate in node 611 and maintained it in node 645.

5.2.2. IEEE 34-node network (Case Study 2)

The Pareto curve of the 34-node feeder is represented in Figure 8, for non-dominated solutions. Figure 8 details the three points chosen to be analyzed and compared with the system values before optimization.

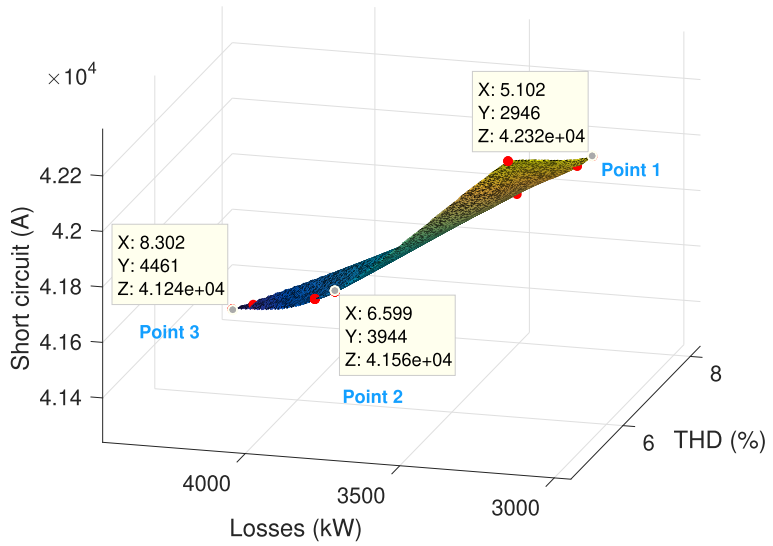

Figure 8: Pareto Curve for the 34-node Network with the chosen points

The chosen points are compared with the initial values of the system. The comparison of the optimization values with the initial values are shown in Table 5 and Table 6 details the number of devices allocated at each chosen point.

Table 5: Comparison of values with and without optimization in the 34-node network

Parameters	Without Optimization (Case Base 2)	MOGWO					
		Point 1	Reduction	Point 2	Reduction	Point 3	Reduction
THD(%)	8.79	5.1	41.98%	6.966	20.75%	8.3	5.57%
Loss(kW)	4591.5	2946.41	35.83%	3981.83	13.28%	4461.48	2.83%
S. circuit(A)	43751	42322.5	3.27%	41519.59	5.10%	41240	5.74%

Table 6: Number of devices allocated at each chosen point in the 34-node network

Devices	Point 1	Point 2	Point 3
DGs	6	6	4
CBs	3	3	3
FCLs	3	5	5

The largest reductions presented in Table 5 for the analysis of losses and harmonic distortion rate, are associated with a greater amount of DG allocation at points 1 and 2. On the other hand, the reduction of the short-circuit current is linked to a greater amount of FCLs allocation.

The harmonic distortion rate gets a greater reduction at point 1 due to less amount of FCLs. This is due to the fact that the FCLs and CBs together create a resonant circuit that causes an increase in the harmonic distortion rate, as can be seen in points 2 and 3, which present lower harmonic distortion rates when compared to point 1.

The amount of FCLs also influences the system losses. Losses at the point are lower due to the lower amount of FCLs and are higher at points 2 and 3 due to the higher amount of FCLs. In view of this, it is observed that despite the increase in losses at points 2 and 3, there was a reduction compared to the initial values of the system.

Next, it is important to analyze the impacts that the allocation of DGs, CBs and FCLs have on each node of the network, so Figure 9 illustrates single-phase fault current in the 34-node network.

Figure 9 shows that some nodes obtained values higher than the initial values, such as node 890, which obtained a greater increase in relation to the others at point 1. It is worth mentioning that, due to the fact that the objective function calculates the average of the three-phase and single-phase faults in each node, it appears that the reduction of the three-phase fault current values had a greater contribution to the minimization of the average of the fault currents.

Figures 10 and 11 illustrate the losses and harmonic distortion rate of the 34-node network, respectively. From Figure 10 it is possible to verify that, at some times of the day, the analyzed points presented values equal to the initial values of the network. However, in some points it is possible to verify that there was a greater reduction of losses in point 1 in relation to points 2 and 3, this fact is associated with the greater amount of FCLs allocated in points 2 and 3.

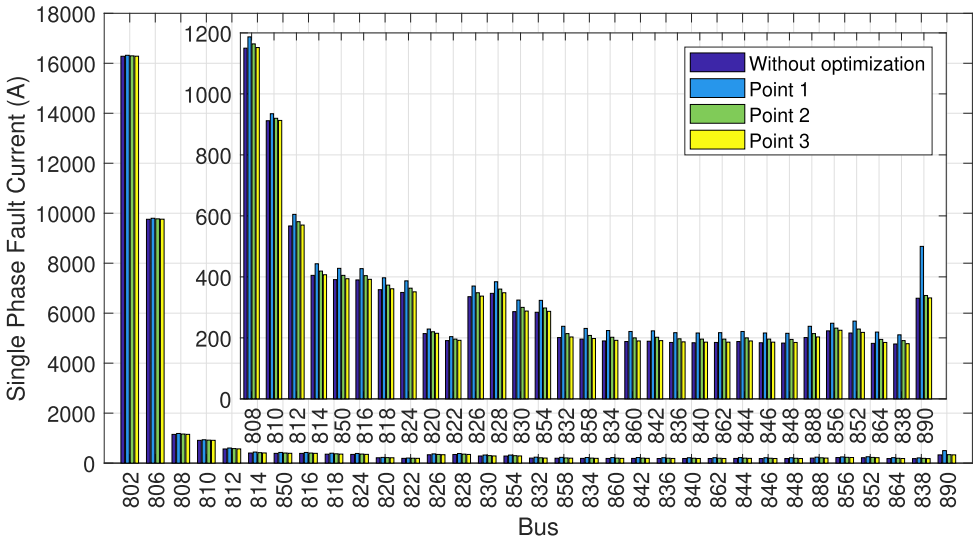

Figure 9: Single-Phase Fault Current in the 34-node Network

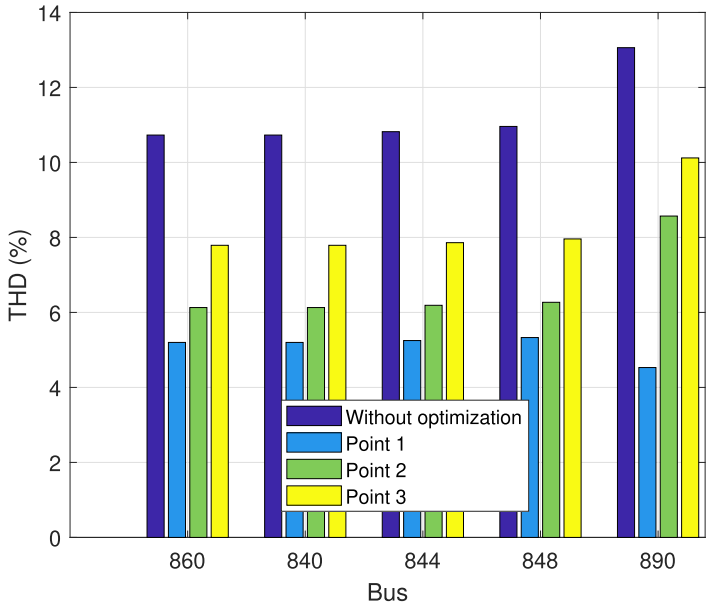

Figure 11: Average daily harmonic distortion rate on the 34-node network

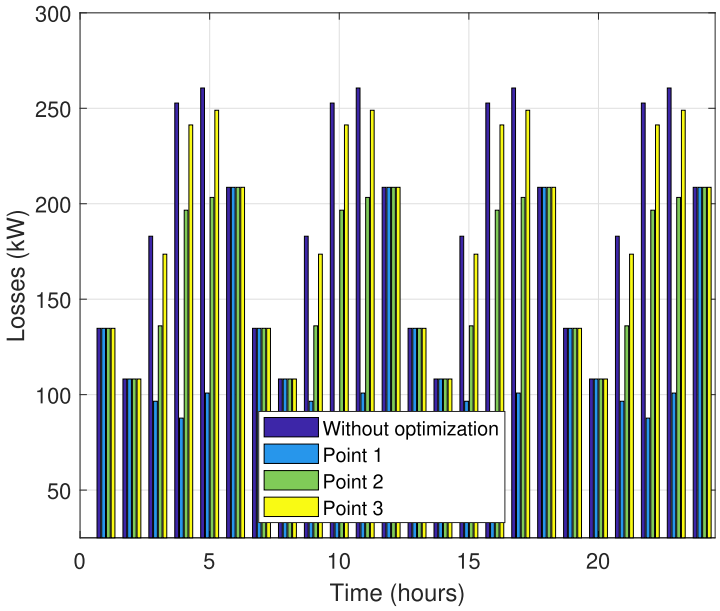

Figure 10: Daily losses on the 34-node network

Figure 11, details the harmonic distortion rate in the 34-node network loads that are not distributed and it can be seen that in all analyzed cases there was a reduction in the harmonic distortion rate when compared to the initial value of the network . It is worth noting that point 1 obtained a greater reduction than points 2 and 3.

5.2.3. IEEE 123-node network (Case Study 3)

Similarly to the simulations of Case Study 1 and Case Study 2, after the simulation of the 123-node feeder (Case Base 3), the Pareto curve was obtained and the three points chosen to be analyzed and compared with the system values before the optimization are summarized in Table 7.

Table 7: Comparison of values with and without optimization in the 123-node network

Parameters	Without Optimization (Case Base 3)	MOGWO					
		Point 1	Reduction	Point 2	Reduction	Point 3	Reduction
THD(%)	10.19	9.54	6.38%	9.63	5.51%	9.89	2.94%
Loss(kW)	1609.8	1384.48	14.00%	1391.50	13.56%	1402.63	12.87%
S. circuit(A)	532641	521819.5	2.03%	521761.59	2.04%	521703	2.05%

When analyzing the 7 Table, it is verified that there was a reduction in

all parameters analyzed in the network. Table 8 quantitatively details the elements that were allocated in the 123-node network for each chosen point.

Table 8: Number of Devices allocated in the 123-node network

Devices	Point 1	Point 2	Point 3
DGs	19	17	10
CBs	22	24	18
FCLs	34	31	18

Losses were reduced at all analyzed points and it is noted that the smallest reduction occurred at point 3 due to the small amount of capacitor bank allocated at this point. At the other points, the amount of capacitor bank allocated manages to supply the increase in losses caused by the existence of a greater number of RLCs. Figure 12 illustrates the network losses of 123 nodes in a 24-hour period.

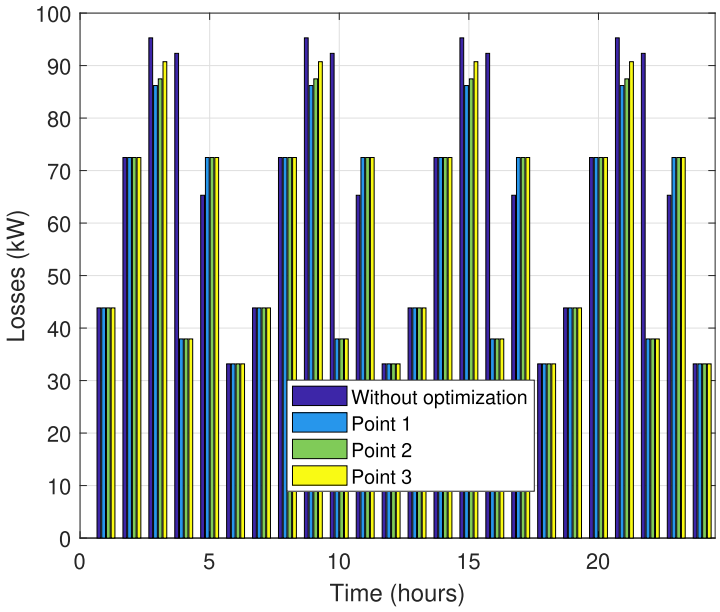

Figure 12: Daily network losses of 123 nodes

Regarding the harmonic distortion rate, it is noted that at point 1 there was the greatest reduction and at point 3 there was a smaller reduction.

These differences are associated not only with the number of devices allocated at each point, but also with the location of these devices throughout the system. Figure 13 details the average daily harmonic distortion rate of the 123-node feeder nodes. From the Figure, it is possible to verify that the average harmonic distortion rate of all nodes were reduced and, again, point 1 obtained better reductions than points 2 and 3 in all analyzed nodes. In addition, point 3 obtained values higher than the values of points 1 and 2 in some nodes. Despite this observed difference, all points presented values lower than the initial values of the network.

Finally, it is worth mentioning that the algorithm was tested and also had a high performance with different load and irradiance profiles using the same 3 IEEE test networks, i.e., showing its robustness in different scenarios.

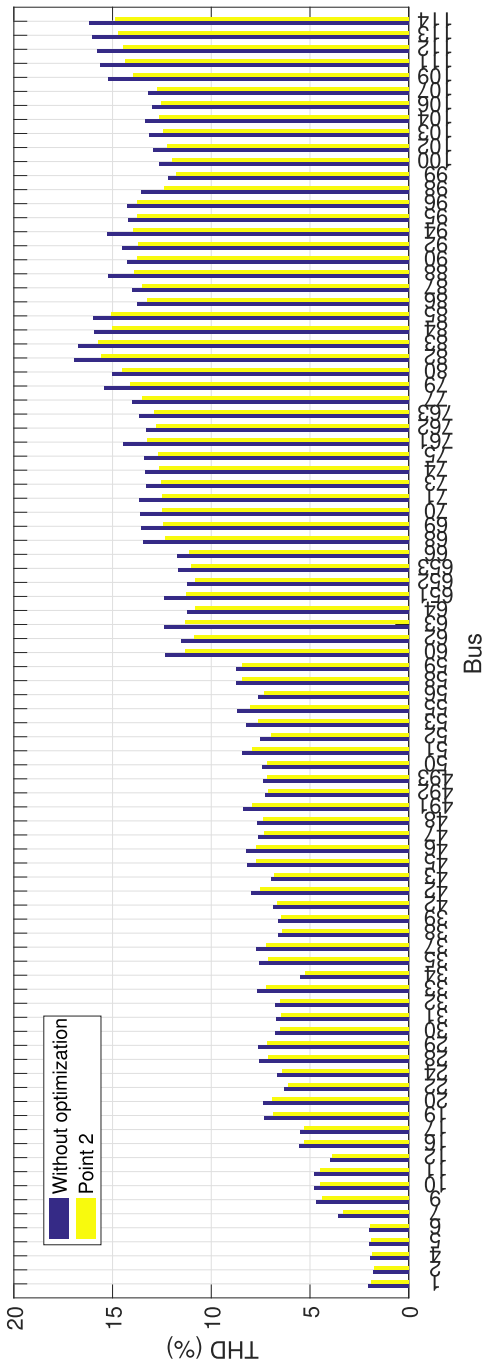

Figure 13: Harmonic Distortion Rate in the network of 123 after the simulation

6. Conclusion

The correct insertion of distributed generation (DG) is important to obtain all the positive impacts that these elements can provide to the system. They can lead to reductions in losses and better energy quality indices. However, its wrong allocation can cause an increase in losses, change in short-circuit current and harmonic distortion rate. These changes also influence the allocation of devices such as capacitor banks and fault current limiters, which were objects of study in this research work. So, this paper proposes a new methodology for optimal allocation of photovoltaic distributed generation, capacitor bank, and fault current limiters in order to simultaneously reduce short-circuit current, losses and harmonic distortion rate through the Multi-objective Gray Wolf Optimizer, allowed to reach satisfactory time limits to simulate in three case study.

The results that correspond to the IEEE 13-node network show that it is the network that obtained the best reductions in the harmonic distortion rate, although the 4.56% increase in the short-circuit current at point 1 and the increase of 8.39% of losses at point 3. Moreover, the 34-node network fulfilled the best loss reductions, compared with the other studied networks. In addition, the large amount of loads distributed in the network only allowed the analysis of only five nodes in the simulation referring to the optimization of the average harmonic distortion rate. Regarding the 123-node network, the greatest reductions occurred in losses and the short-circuit current suffered the smallest reduction when compared to the 13 and 34-node networks. It also stood out for obtaining voltage values within the appropriate voltage range, unlike what was observed in the 13 and 34 node networks. Finally, following the results, the choice of the optimum number and the location of elements allocated and deliver good operating option for the system related with short-circuit current, losses and harmonic distortion rate.

As future work, it is envisaged to include in the modeling of the problem the allocation of protection devices in the network, the use of other DG sources (such as wind power), the inclusion of energy storage elements (battery banks), and the active filters to enhance THD correction.

Acknowledgment

This work was partially supported by CNPq 309737/2021-4, FAPES 2022-BWBR2, 2021-WMR44 and NiDA Project. Professor Yahyaoui is funded by PROEMRED Project M3010 by the university Rey Juan Carlos, Spain.

References

[1] M. Soshinskayaa, W. H.J., Crijns-Grausa, J. M.GuerrerobJuan, C.Vasquezb, Microgrids: Experiences, barriers and success factors, Renewable and Sustainable Energy Reviews 40 (2014) 659–672.

[2] J. F. Fardin, H. R. de Oliveira Rocha, C. B. Donadel, R. Fiorotti, Distributed generation energy in relation to renewable energy: Principle, techniques, and case studies, in: Advances in Renewable Energies and Power Technologies, Elsevier, 2018, pp. 345–375.

[3] R. Fiorotti, J. Fardin, L. Encarnacao, C. Donadel, A novel strategy for distribution network reinforcement planning considering the firm capacity of distributed generation units, IEEE Latin America Transactions 17 (04) (2019) 530–539.

[4] R. Walling, R. Saint, R. Dugan, J. Burke, L. Kojovic, Summary of distributed resources impact on power delivery systems, IEEE Transactions on Power Delivery 10 (7) (2016) 873–884.

[5] K. Balamurugan, D. Srinivasan, T. Reind, Impact of distributed generation on power distribution systems, Energy Procedia 25 (2012) 93–100.

[6] S.-E. Razavi, E. Rahimi, M. S. Javadi, A. E. Nezhad, M. Lotfi, M. Shafiekhah, J. P. Catalão, Impact of distributed generation on protection and voltage regulation of distribution systems: A review, Renewable and Sustainable Energy Reviews 105 (2019) 157–167.

[7] M. C.Vargas, M. A. Mendes, O. E. Batista, Impacts of high pv penetration on voltage profile of distribution feeders under brazilian electricity regulation, 13th IEEE International Conference on Industry Applications (2018).

[8] L.-H. Chen, Overcurrent protection for distribution feeders with renewable generation, International Journal of Electrical Power Energy Systems 84 (ISSN 0142-0615) (2017) 202–213.

[9] D. Fallows, S. Nuzzo, A. Costabeber, M. Galea, Harmonic reduction methods for electrical generation: a review, IET Generation, Transmission Distribution (2018).

[10] E. A. Al-Ammar, G. A. Ghazi, W. Ko, Y. Khan, A. Beroual, J. Hong, S.-H. Song, Comprehensive impact analysis of ambient temperature on multi-objective capacitor placements in a radial distribution system, Ain Shams Engineering Journal (2020).

[11] J. Urbanský, Beňa, V. Krištof, M. Hvizdoš, Duplex reactor - forgotten element to reduce short-circuit currents, in: 2020 21st International Scientific Conference on Electric Power Engineering (EPE), 2020, pp. 1–4.

[12] A. Rahiminejad, S. H. Hosseinian, B. Vahidi, S. Shahrooyan, Simultaneous distributed generation placement, capacitor placement, and reconfiguration using a modified teaching-learning-based optimization algorithm, Electric Power Components and Systems 44 (14) (2016) 1631–1644.

[13] S. Ouali, A. Cherkaoui, Optimal allocation of combined renewable distributed generation and capacitor units for interconnection cost reduction, Journal of Electrical and Computer Engineering (2020).

[14] A. Bayat, A. Bagheri, Optimal active and reactive power allocation in distribution networks using a novel heuristic approach, Applied Energy 233 (2019) 71–85.

[15] S. Ouali, A. Cherkaoui, Optimal allocation of combined renewable distributed generation and capacitor units for interconnection cost reduction, Journal of Electrical and Computer Engineering, Article ID 5101387 (2020) 1–11.

[16] A. A. Augusto, J. C. S. de Souza, M. B. Do Coutto Filho, H. R. de Oliveira Rocha, J. E. V. Tafur, Optimized capacitor placement considering load and network variability, Journal of Control, Automation and Electrical Systems 31 (6) (2020) 1489–1498.

[17] A. M. Shaheen, R. A. El-Sehiemy, Optimal coordinated allocation of distributed generation units/capacitor banks/voltage regulators by egwa, IEEE Systems Journal 15 (1) (2020) 257–264.

[18] C. Venkatesan, R. Kannadasan, M. H. Alsharif, M.-K. Kim, J. Nebhen, A novel multiobjective hybrid technique for siting and sizing of dis-

tributed generation and capacitor banks in radial distribution systems, Sustainability 13 (6) (2021) 3308.

[19] L. Zhang, C. Shen, Y. Chen, S. Huang, W. Tang, Coordinated allocation of distributed generation, capacitor banks and soft open points in active distribution networks considering dispatching results, Applied energy 231 (2018) 1122–1131.

[20] I. A. Quadri, S. Bhowmick, D. Joshi, A comprehensive technique for optimal allocation of distributed energy resources in radial distribution systems, Applied energy 211 (2018) 1245–1260.

[21] M. T. Mouwafi, R. A. El-Sehiemy, A. A. Abou El-Ela, A two-stage method for optimal placement of distributed generation units and capacitors in distribution systems, Applied Energy 307 (2022) 118188.

[22] A. Naderipour, Z. Abdul-Malek, M. Hajivand, Z. M. Seifabad, M. A. Farsi, S. A. Nowdeh, I. F. Davoudkhani, Spotted hyena optimizer algorithm for capacitor allocation in radial distribution system with distributed generation and microgrid operation considering different load types, Scientific reports 11 (1) (2021) 1–15.

[23] L. D. Pereira, I. Yahyaoui, R. Fiorotti, L. S. de Menezes, J. F. Fardin, H. R. Rocha, F. Tadeo, Optimal allocation of distributed generation and capacitor banks using probabilistic generation models with correlations, Applied Energy 307 (2022) 118097.

[24] M. E. Hamidi, R. M. Chabanloo, Optimal allocation of distributed generation with optimal sizing of fault current limiter to reduce the impact on distribution networks using nsga-ii, IEEE Systems journal 13 (2) (2018) 1714–1724.

[25] A. Mahmoudian, M. Niasati, M. A. Khanesar, Multi objective optimal allocation of fault current limiters in power system, International Journal of Electrical Power & Energy Systems 85 (2017) 1–11.

[26] A. A. A. El-Ela, R. A. El-Sehiemy, A. M. Shaheen, A. R. Ellien, Optimal allocation of distributed generation units correlated with fault current limiter sites in distribution systems, IEEE Systems Journal 15 (2) (2020) 2148–2155.

[27] L. F. S. Azeredo, I. Yahyaoui, R. Fiorotti, J. F. Faradin, H. Garcia-Pereira, H. R. de Oliveira Rocha, Multi-objective gray wolf optimization for distribuited generation, capacitors banks and fault current limiters allocation, in: 2023 Annual Seminar of Automatics, Industrial Electronics and Instrumentation, 2023, pp. 1–6.

[28] V. Bhadoria, N. Singh, V. Shrivastava, A review on distributed generation definitions and dg impacts on distribution system, 2013.

[29] M. Pehnt, B. Praetorius, Micro Cogeneration, Physica-Verlag HD, Heidelberg, 2009, pp. 45–75.

[30] A. Eltamaly, Y. Mohamed, A.-H. Ahmed, A. A. Elghaffar, Impact of distributed generation (dg) on the distribution system network, International Journal of Engineering Science (04 2019).

[31] P. P. Barker, R. W. D. Mello, Determining the impact of distributed generation on power systems. i. radial distribution systems, in: 2000 Power Engineering Society Summer Meeting (Cat. No.00CH37134), Vol. 3, 2000, pp. 1645–1656 vol. 3.

[32] R. C. Dugan, T. E. McDermott, Operating conflicts for distributed generation on distribution systems, in: 2001 Rural Electric Power Conference. Papers Presented at the 45th Annual Conference (Cat. No.01CH37214), 2001, pp. A3/1–A3/6.

[33] V. H. M. Quezada, J. R. Abbad, T. G. S. Roman, Assessment of energy distribution losses for increasing penetration of distributed generation, IEEE Transactions on Power Systems 21 (2) (2006) 533–540.

[34] P. Radatz, C. Rocha, W. Sunderman, M. Rylander, J. Peppanen, Opendss pvsystem and invcontrol element models (2020).

[35] R. C. Dugan, Opendss manual (2016).
URL `http://sourceforge.net/p/electricdss/code/HEAD/tree/trunk/Distrib/Doc/OpenDSSManual.pdf`

[36] R. C. Dugan, Dss fault current calculation procedures (2003).

[37] C. M. Fonseca, P. J. Fleming, An overview of evolutionary algorithms in multiobjective optimization, Evolutionary Computation 3 (1) (1995) 1–16.

[38] S. Mirjalili, S. M. Mirjalili, A. Lewis, Grey wolf optimizer, Advances in Engineering Software 69 (2014) 46 – 61.

[39] S. Mirjalili, S. Saremi, S. M. Mirjalili, L. dos S. Coelho, Multi-objective grey wolf optimizer: A novel algorithm for multi-criterion optimization, Expert Systems with Applications 47 (2016) 106 – 119.

[40] P. Jangir, R. Bhesdadiya, D. Ladumor, I. Trivedi, A multi-objective grey wolf optimization algorithm for economic/environmental dispatch, PNFE-2016At: St. Peters Engineering college, Hyderabad, India (2016).

[41] IEEE, Ieee standard for shunt power capacitors, IEEE Std 18-2012 (2013) 1–39.

[42] W. H. Kersting, Radial distribution test feeders, IEEE Transactions on Power Delivery (2011) 908–912.

[43] J. Zou, Q. Li, S. Yang, H. Bai, J. Zheng, A prediction strategy based on center points and knee points for evolutionary dynamic multi-objective optimization, Applied soft computing 61 (2017) 806–818.